Evaluating the coherence and time-domain profile of quantum cascade laser frequency combs

David Burghoff,[1,*] **Yang Yang,**[1] **Darren J. Hayton,**[2] **Jian-Rong Gao,**[2,3] **John L. Reno,**[4] **and Qing Hu**[1]

[1]*Department of Electrical Engineering and Computer Science, Research Laboratory of Electronics, Massachusetts Institute of Technology, Cambridge, Massachusetts 02139, USA*
[2]*SRON Netherlands Institute for Space Research, 9747 AD, Groningen, Netherlands*
[3]*Kavli Institute of NanoScience, Delft University of Technology, Lorentzweg 1, 2628 CJ Delft, The Netherlands*
[4]*Center for Integrated Nanotechnology, Sandia National Laboratories, Albuquerque, New Mexico 87123, USA*
[*]*burghoff@mit.edu*

Abstract: Recently, much attention has been focused on the generation of optical frequency combs from quantum cascade lasers. We discuss how fast detectors can be used to demonstrate the mutual coherence of such combs, and present an inequality that can be used to quantitatively evaluate their performance. We discuss several technical issues related to shifted wave interference Fourier Transform spectroscopy (SWIFTS), and show how such measurements can be used to elucidate the time-domain properties of such combs, showing that they can possess signatures of both frequency-modulation and amplitude-modulation.

References and links

1. A. Hugi, G. Villares, S. Blaser, H. C. Liu, and J. Faist, "Mid-infrared frequency comb based on a quantum cascade laser," Nature **492**(7428), 229-233 (2012).
2. D. Burghoff, T.-Y. Kao, N. Han, C. W. I. Chan, X. Cai, Y. Yang, D. J. Hayton, J.-R. Gao, J. L. Reno, and Q. Hu, "Terahertz laser frequency combs," Nat. Photonics **8**(6), 462-467 (2014).
3. G. Villares, A. Hugi, S. Blaser, and J. Faist, "Dual-comb spectroscopy based on quantum-cascade-laser frequency combs," Nat Commun **5**, 5192 (2014).
4. Y. Wang, M. G. Soskind, W. Wang, and G. Wysocki, "High-resolution multi-heterodyne spectroscopy based on Fabry-Perot quantum cascade lasers," Appl. Phys. Lett. **104**(3), 031114 (2014).
5. S. Bartalini, L. Consolino, P. Cancio, P. De Natale, P. Bartolini, A. Taschin, M. De Pas, H. Beere, D. Ritchie, M. S. Vitiello, and R. Torre, "Frequency-comb-assisted terahertz quantum cascade laser spectroscopy," Phys. Rev. X **4**, 021006 (2014).
6. N. Han, A. de Geofroy, D. P. Burghoff, C. W. I. Chan, A. W. M. Lee, J. L. Reno, and Q. Hu, "Broadband all-electronically tunable MEMS terahertz quantum cascade lasers," Opt. Lett. **39**(12), 3480-3483 (2014).
7. A. W. Lee, T.-Y. Kao, D. Burghoff, Q. Hu, and J. L. Reno, "Terahertz tomography using quantum-cascade lasers," Opt. Lett. **37**(2), 217-219 (2012).
8. S. Barbieri, M. Ravaro, P. Gellie, G. Santarelli, C. Manquest, C. Sirtori, S. P. Khanna, E. H. Linfield, and A. G. Davies, "Coherent sampling of active mode-locked terahertz quantum cascade lasers and frequency synthesis," Nat. Photonics **5**(5), 306-313 (2011).
9. J. B. Khurgin, Y. Dikmelik, A. Hugi, and J. Faist, "Coherent frequency combs produced by self frequency modulation in quantum cascade lasers," Appl. Phys. Lett. **104**(8), 081118 (2014).

10. P. Del'Haye, A. Schliesser, O. Arcizet, T. Wilken, R. Holzwarth, and T. J. Kippenberg, "Optical frequency comb generation from a monolithic microresonator," Nature **450**(7173), 1214-1217 (2007).
11. D. Burghoff, T.-Y. Kao, D. Ban, A. W. M. Lee, Q. Hu, and J. Reno, "A terahertz pulse emitter monolithically integrated with a quantum cascade laser," Appl. Phys. Lett. **98**(6), 061112 (2011).
12. S. S. Dhillon, C. Sirtori, J. Alton, S. Barbieri, A. de Rossi, H. E. Beere, and D. A. Ritchie, "Terahertz transfer onto a telecom optical carrier," Nat. Photonics **1**(7), 411-415 (2007).
13. M. Rösch, G. Scalari, M. Beck, and J. Faist, "Octave-spanning semiconductor laser," Nat. Photonics **9**(1), 42-47 (2015).
14. D. Bachmann, M. Rösch, C. Deutsch, M. Krall, G. Scalari, M. Beck, J. Faist, K. Unterrainer, and J. Darmo, "Spectral gain profile of a multi-stack terahertz quantum cascade laser," Appl. Phys. Lett. **105**(18), 181118 (2014).
15. F. Ferdous, H. Miao, D. E. Leaird, K. Srinivasan, J. Wang, L. Chen, L. T. Varghese, and A. M. Weiner, "Spectral line-by-line pulse shaping of on-chip microresonator frequency combs," Nat. Photonics **5**(12), 770-776 (2011).
16. S. B. Papp and S. A. Diddams, "Spectral and temporal characterization of a fused-quartz-microresonator optical frequency comb," Phys. Rev. A **84**(5), 053833 (2011).
17. M. Wienold, B. Röben, L. Schrottke, and H. T. Grahn, "Evidence for frequency comb emission from a Fabry-Pérot terahertz quantum-cascade laser," Opt. Express **22**(25), 30410-30424 (2014).
18. V. Torres-Company, D. Castelló-Lurbe, and E. Silvestre, "Comparative analysis of spectral coherence in microresonator frequency combs," Opt. Express **22**(4), 4678-4691 (2014).
19. L. Mandel and E. Wolf, "Coherence properties of optical fields," Rev. Mod. Phys. **37**(2), 231-287 (1965).
20. D. P. Burghoff, "Broadband terahertz photonics," Thesis, Massachusetts Institute of Technology (2014).
21. W. Zhang, P. Khosropanah, J. R. Gao, E. L. Kollberg, K. S. Yngvesson, T. Bansal, R. Barends, and T. M. Klapwijk, "Quantum noise in a terahertz hot electron bolometer mixer," Appl. Phys. Lett. **96**(11), 111113 (2010).
22. E. Langford, N. Schwertman, and M. Owens, "Is the property of being positively correlated transitive?" Am. Stat. **55**(4), 322-325 (2001).
23. M. C. Wanke, A. D. Grine, C. T. Fuller, C. D. Nordquist, M. J. Cich, J. L. Reno, and M. Lee, "Common mode frequency instability in internally phase-locked terahertz quantum cascade lasers," Opt. Express **19**(24), 24810-24815 (2011).
24. P. Gellie, S. Barbieri, J.-F. Lampin, P. Filloux, C. Manquest, C. Sirtori, I. Sagnes, S. P. Khanna, E. H. Linfield, A. G. Davies, H. Beere, and D. Ritchie, "Injection-locking of terahertz quantum cascade lasers up to 35 GHz using RF amplitude modulation," Opt. Express **18**(20), 20799-20816 (2010).
25. S. Barbieri, W. Maineult, S. S. Dhillon, C. Sirtori, J. Alton, N. Breuil, H. E. Beere, and D. A. Ritchie, "13 GHz direct modulation of terahertz quantum cascade lasers," Appl. Phys. Lett. **91**(14), 143510 (2007).
26. T. Herr, K. Hartinger, J. Riemensberger, C. Y. Wang, E. Gavartin, R. Holzwarth, M. L. Gorodetsky, and T. J. Kippenberg, "Universal formation dynamics and noise of Kerr-frequency combs in microresonators," Nat. Photonics **6**(7), 480-487 (2012).
27. L. Consolino, A. Taschin, P. Bartolini, S. Bartalini, P. Cancio, A. Tredicucci, H. E. Beere, D. A. Ritchie, R. Torre, M. S. Vitiello, and P. De Natale, "Phase-locking to a free-space terahertz comb for metrological-grade terahertz lasers," Nat Commun **3**, 1040 (2012).
28. J. Maysonnave, N. Jukam, M. S. M. Ibrahim, R. Rungsawang, K. Maussang, J. Mado, P. Cavali, P. Dean, S. P. Khanna, D. P. Steenson, E. H. Linfield, A. G. Davies, S. S. Dhillon, and J. Tignon, "Measuring the sampling coherence of a terahertz quantum cascade laser," Opt. Express **20**(15), 16662-16670 (2012).
29. P. Friedli, H. Sigg, B. Hinkov, A. Hugi, S. Riedi, M. Beck, and J. Faist, "Four-wave mixing in a quantum cascade laser amplifier," Appl. Phys. Lett. **102**(22), 222104 (2013).

1. Introduction

Frequency comb sources based on quantum cascade lasers (QCLs) have attracted much attention since their initial demonstration in 2012 [1]. Such combs have been demonstrated in both the mid-infrared [1] and terahertz (THz) [2], and offer much promise as sources for compact multi-heterodyne spectroscopy [3, 4], as frequency references for high-resolution spectroscopy [5] using tunable lasers [6], or as broadband sources for terahertz tomography [7]. From a fundamental physics perspective, QCLs are also interesting in that they cannot only operate in regimes resembling traditional mode-locked lasers [8], but can also act in a regime of self-frequency modulation [9] that more closely resembles the output of microresonator frequency combs [10]. The latter regime can be interpreted as resulting from the $\chi^{(3)}$ nonlinearity: the otherwise unevenly-spaced lines of a multi-mode laser are injection-locked through four-wave mixing to form a uniform comb. Alternatively, this can be construed as traditional microresonator comb formation, with the laser gain compensating the cold-cavity losses and sponta-

neous emission acting as the pump. This process will occur in any broadband laser with a sufficiently large $\chi^{(3)}$ nonlinearity and sufficiently low group velocity dispersion—whether that dispersion is low because of dispersion engineering [2, 11, 12] or because of band-structure engineering [1, 13, 14].

The key aspect that determines whether a QCL is acting as a multi-mode laser or as a frequency comb is the coherence of the output: in an incoherent multi-mode laser the phase of each line is uncorrelated, while in a frequency comb there is a definite phase relation that exists between the lines. (This is in contrast to traditional microcombs, in which four-wave mixing also gives rise to a noticeable broadening of the optical spectrum.) Equivalently, the lines of a multi-mode laser are not uniformly spaced, while the lines of a frequency comb are. Clearly, characterizing the temporal coherence of QCL combs is of utmost importance. In traditional microresonator combs, coherence has been assessed by line-by-line pulse shaping, in which the comb lines' phases are individually adjusted to produce a minimum-width time-domain pulse, assessed using autocorrelation [15, 16]. This approach is problematic in QCL combs for a number of reasons, chiefly that autocorrelators and spatial light modulators are difficult to produce at long wavelengths. Instead, coherence of QCL combs has been primarily evaluated using a number of techniques centered on the beatnote produced by combs on sufficiently fast optical detectors, as measured through a Fourier transform spectrometer (FTS). These techniques include intermode beat spectroscopy [1], a technique that examines the shape of the beatnote as a function of FTS delay, shifted wave interference FTS (SWIFTS), a technique that examines the I/Q-demodulated beatnote [2], and techniques based on self-mixing within the QCL [17]. (It is also possible to assess coherence by beating two combs together, although this of course requires two nearly identical lasers [3].) To some extent, these techniques have all revolved around using the beatnote to produce spectra that resemble the power spectrum and noting that they are similar. However, for comparative analysis it is necessary to develop a formalism capable of quantitatively describing the degree of coherence. In this paper we present such a definition and show that the SWIFTS technique directly measures this degree of coherence with a quantitative metric. We also show that SWIFTS can be used to gain almost as much information as line-by-line pulse shaping, and can be used to directly extract the time-dependent intensity and time-dependent frequency.

2. Degree of mutual coherence

2.1. Coherence of two lines

For simplicity and to illustrate the essential, we consider a prototypical coherence detector, shown in Fig. 1(a), that is capable of measuring the mutual coherence of two lines. Two beams at different optical frequencies, ω_1 and ω_2, are shined onto a single detector fast enough to detect their optical beatnote. The resulting signal is then electronically mixed with a local oscillator (LO) whose frequency ω_0 is near the difference frequency of the two lines, $\omega_{21} = \omega_2 - \omega_1$. If each quadrature of the local oscillator is mixed with the beatnote, then the two signals produced—denoted by $S_I(t)$ and $S_Q(t)$—can be interpreted as producing a complex analytic $S_\pm(t) \equiv S_I(t) \mp iS_Q(t)$. If the optical fields have the form $E_1(t)e^{i\omega_1 t}$ and $E_2(t)e^{i\omega_2 t}$, then the detected analytic signal $S_+(t)$ takes the form

$$S_+(t) = E_1^*(t)E_2(t)e^{i(\omega_{21} - \omega_0)t}. \tag{1}$$

Note that when the phasors $E_1(t)$ and $E_2(t)$ are fixed in time and have a frequency difference equal to the local oscillator's frequency, the analytic signal $S_+(t)$ will be a finite DC signal. However, if there is a fluctuating phase relation between E_1 and E_2, then the phase of the measured analytic signal will also fluctuate. Likewise, if the frequency difference ω_{21} differs
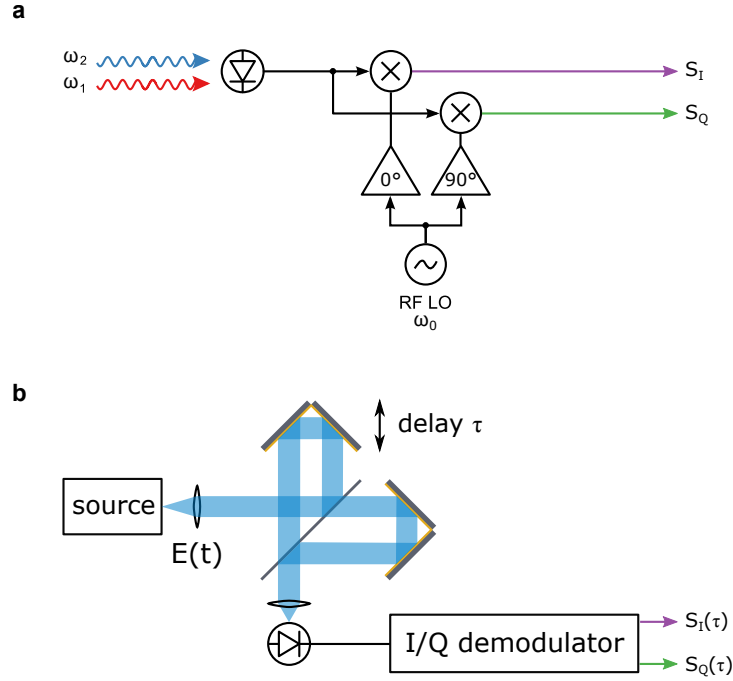
a

b

Fig. 1. (a) A "coherence detector," a system capable of detecting the mutual coherence of two lines with respect to a local oscillator (LO). (b) A coherence detector placed at the output of an FTS, performing SWIFTS. The LO for the demodulator is discussed in Section 3.1.

from the local oscillator frequency ω_0, then the phase of the analytic signal will also change, albeit in a simple way. If one specifies an integration time over which the analytic signal is measured (i.e., a gate time), then the magnitude of the measured analytic signal, $|\langle S_+(t)\rangle|$, represents the degree to which the fields are phase stable and separated by the LO frequency. In fact, by the well-known Cauchy-Schwarz inequality, it must be the case that

$$0 \le \left| \left\langle E_1^*(t)E_2(t)e^{i(\omega_{21}-\omega_0)t} \right\rangle \right|^2 \le \left\langle |E_1(t)|^2 \right\rangle \left\langle |E_2(t)|^2 \right\rangle, \tag{2}$$

which means that we can rigorously define a normalized coherence $g_{21}(\omega_0)$ as

$$g_{21}(\omega_0) \equiv \frac{\left\langle E_1^*(t)E_2(t)e^{i(\omega_{21}-\omega_0)t} \right\rangle}{\sqrt{\left\langle |E_1(t)|^2 \right\rangle \left\langle |E_2(t)|^2 \right\rangle}} \tag{3}$$

The numerator of Eq. (3) is the measured analytic signal, while the denominator represents a normalization to the intensity of each line. By Eq. (2), the magnitude of the normalized coherence must fall between 0 and 1, with $|g_{21}| = 0$ representing complete incoherence and $|g_{21}| = 1$ representing complete coherence. Similar definitions abound for the description of first-order coherence [18, 19], but this one in particular is useful because it is directly accessible by measurement. Note that the degree of coherence is dependent on the choice of LO frequency: an LO frequency detuned from the optical frequency difference by more than the inverse of the gate time will yield a zero result. In addition, the phase of the normalized coherence represents the average phase difference between the two lines.

2.2. Generalization to multiple lines

In reality, a frequency comb has many lines whose coherence must be assessed, but the generalization of the figure of merit to the multiple lines of a frequency comb is straightforward. We define the degree of coherence between lines i and j with respect to the LO frequency ω_0 as

$$g_{ji}(\omega_0) \equiv \frac{\left\langle E_i^*(t)E_j(t)e^{i(\omega_{ji}-\omega_0)t}\right\rangle}{\sqrt{\left\langle |E_i(t)|^2\right\rangle \left\langle |E_j(t)|^2\right\rangle}}. \tag{4}$$

Though this definition unfolds naturally, it is challenging to measure. First of all, a source with N lines will possess N^2 pairs of coherences. (g_{ji} essentially represents a normalized covariance matrix, and is analogous to the density matrix in quantum mechanics.) Though one could in principle filter each line individually, e.g. using a grating, this would be extremely tedious. Instead, we mainly focus on the coherence of nearby lines, defined by

$$g_{\pm}(\omega,\omega_0) \equiv \frac{\left\langle E^*(\omega)E(\omega\pm\omega_0)\right\rangle}{\sqrt{\left\langle |E(\omega)|^2\right\rangle \left\langle |E(\omega\pm\omega_0)|^2\right\rangle}}. \tag{5}$$

Nevertheless, just as a single detector element is insufficient for determining the power spectrum of a source, a simple coherence detector is not enough to determine the coherence of a broad spectrum: some spectral selectivity mechanism needs to be present. Each of the techniques that rely on measuring the radio frequency (RF) beatnote through an interferometer measure this coherence spectrum to varying degrees. In SWIFTS, this is accomplished by placing a coherence detector at the output of an interferometer, shown in Fig. 1(b). Though ω_0 is usually chosen to be the repetition rate of the frequency comb, $\Delta\omega$, this does not actually need to be the case provided a stable phase reference is available. It is also possible to investigate pairs beyond nearest-neighbor (e.g., $2\Delta\omega$) provided the detector has sufficient bandwidth. Note that intermode beatnote spectroscopy can be considered a special case of SWIFTS, in which only the magnitude of the analytic signal is found and ω_0 is swept by a spectrum analyzer. In any case, the interferometric part of the transmitted optical power is found using $P(t) = (E(t)+E(t-\tau))^2 \sim E(t)E(t-\tau)$, where τ is the delay imparted by the FTS's translation element. Suppose that we measure both RF quadratures of the beatnote in addition to the normal DC interferogram. The normal, in-phase, and in-quadrature interferograms can then be expressed respectively as

$$S_0(\tau) = A(\tau)\int_{-\infty}^{\infty} dt\, K(t)E(t)E(t-\tau)$$

$$S_I(\tau,\omega_0) = A(\tau)\int_{-\infty}^{\infty} dt\, K(t)E(t)E(t-\tau)\cos(\omega_0 t) \tag{6}$$

$$S_Q(\tau,\omega_0) = A(\tau)\int_{-\infty}^{\infty} dt\, K(t)E(t)E(t-\tau)\sin(\omega_0 t),$$

where $A(\tau)$ represents the interferometer's apodization function and $K(t)$ represents a measurement kernel, i.e. the effect of integrating over laboratory timescales. As usual, we combine the quadratures into an analytic function $S_{\pm}(\tau,\omega_0) = S_I(\tau,\omega_0) \mp iS_Q(\tau,\omega_0)$; using elementary Fourier analysis one then finds that the corresponding spectra are [20]

$$S_0(\omega) = A(\omega) * [E^*(\omega)\cdot(E*K)(\omega)]$$

$$S_{\pm}(\omega,\omega_0) = A(\omega) * [E^*(\omega)\cdot(E*K)(\omega\pm\omega_0)]. \tag{7}$$

Here, asterisks are used to represent convolution. Typically, the integration kernel $K(\omega)$ is much narrower than the spectra of interest (on the order of Hz, compared with GHz) and can be considered a delta function, in which case one finds that the SWIFTS signal is a product of the electric field at one frequency and the electric field at a frequency shifted by the LO frequency. Though the instrument apodization broadens the resulting spectrum, it does so after the product has been measured, allowing for the coherence to be assessed. In essence, when the separation between two lines differs from ω_0 by more than the bandwidth of $K(\omega)$, their SWIFT spectrum vanishes and their FT spectrum does not. Traditional FTS measures the cross-correlation of the electric field with itself (i.e., the autocorrelation), while SWIFTS measures the cross-correlation of the electric field with a precisely frequency-shifted version of itself.

Once the normal spectrum $S_0(\omega)$ and the SWIFTS spectrum $S_+(\omega) \equiv S_+(\omega, \Delta\omega)$ have been measured, further data processing is required to numerically measure the degree of coherence defined in Eq. (3). Though it might be tempting to simply divide the magnitude of the SWIFTS spectrum $|S_+(\omega)|$ by the power normalization $[S_0(\omega)S_0(\omega + \Delta\omega)]^{1/2}$, strictly speaking this is not correct since all of the measured spectra have been convolved with the apodization function, and this must be undone (that is, deconvolved). Assuming the true spectra consist of discrete lines that are resolved by the interferometer, this problem is well-posed. When this is the case, the line frequencies $\{\omega_i\}$ can be determined by zero-padding the power spectrum to a sufficient degree [13] and least-squares fitting the interferograms to a discrete summation of exponentials with phasors $\{c^{(i)}\}$:

$$S_0(\tau) = \sum_i c_0^{(i)} \exp(i\omega_i\tau)$$
$$S_+(\tau) = \sum_i c_+^{(i)} \exp(i\omega_i\tau). \tag{8}$$

Once the phasors corresponding to each interferogram have been found, the degree of coherence can then be expressed at a particular frequency ω_i by simply calculating the ratio

$$|g(\omega_i)| = \frac{\left|c_+^{(i)}\right|}{\sqrt{c_0^{(i)} c_0^{(i+1)}}}. \tag{9}$$

Figure 2 illustrates the steps of this process for a SWIFTS signal measured from a lens-coupled terahertz comb device characterized in [2]. The comb output was characterized at a bias current of 900 mA, a temperature of 50 K, and using a hot electron bolometer from SRON [21].

First, Fig. 2(a) shows the deconvolved normal interferogram alongside the original normal interferogram. Because the lines of the original spectrum are resolved by the FTS measurement (i.e., multiple copies of the center burst were measured), the deconvolution will not overfit the measurement. Next, Fig. 2(b) plots the deconvolution coefficients as a function of frequency, with the purple line representing the numerator of Eq. (9) and the red line representing the denominator of Eq. (9). Lastly, Fig. 2(c) shows the degree of coherence corresponding to the data in Fig. 2(b). Since the process of division is highly-susceptible to noise, coherence was assessed by locally determining the proportionality constant using a window with a full-width half maximum of 2.5 lines (17 GHz). Nevertheless, significant statistical fluctuations remain in the result, and so a 95% confidence interval is also plotted that takes into account the observed noise.

At the two portions of the gain spectrum where the laser output is largest, the degree of coherence is close to unity. However, as one nears the edge of each portion the coherence spectrum falls off faster than the power spectrum product, which causes the degree of coherence to decay to zero. This can be understood as a consequence of the four-wave mixing process

a **Deconvolution process**

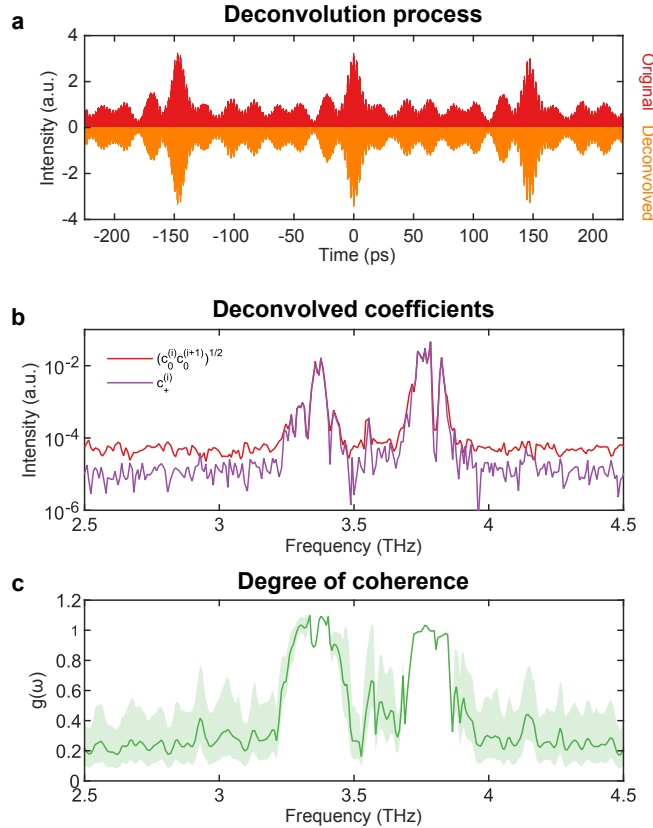**b** **Deconvolved coefficients**

c **Degree of coherence**

Fig. 2. (a) Original normal spectrum interferogram, along with the deconvolved version (fit to Eq. (8)). Close agreement is achieved without overfitting provided that the lines are resolved by the FTS. (b) Magnitude of the deconvolved coefficients. The close agreement between the numerator and denominator of Eq. (9) is the hallmark of a comb. (c) Degree of coherence corresponding to the coefficients shown. The shaded region indicates the 95% confidence interval.

that drives comb formation: weak lines near the edge of the gain spectrum are primarily phase-locked to the comb by similarly weak nearby lines, and so the coherence is reduced. Note that, in general, a proper coherence measurement should always result in a coherence spectrum which is no larger or broader than the power spectrum product, i.e. $|g(\omega)| \leq 1$. In these measurements $|g|$ is occasionally seen to slightly exceed unity, although we attribute this to measurement artifacts that arise from the Fourier domain nature of the measurement.

The major limitation of using interferometric techniques like SWIFTS to assess coherence is that they are unable to easily verify the coherence of distant lines, specifically lines which are separated by more than the detector bandwidth. Though the magnitudes of various lower-order coherences can be used to place bounds on the magnitudes of higher-order ones [22], this constraint is often weak. In particular, if the power spectrum of the comb vanishes between two lines, then no statements can be made about their coherence at all. Since the spectrum of the comb shown above is split into two lobes separated by a spectral gap, the relative offset frequency of each lobe cannot be measured using this technique (and is also not guaranteed to be stable). Another limitation of SWIFTS when compared with a technique like beatnote inter-ferometry, which records an RF spectrum, is that SWIFTS requires a phase reference, which

in turn makes acquiring data at a local oscillator frequency other than the laser's repetition rate more difficult. Though this allows for a clean measurement of the degree of coherence and a reconstruction of the waveform's temporal profile, incoherent light appears only as a departure of the degree of coherence from unity. In other words, using SWIFTS one could easily determine that a pair of lines is not actually spaced by the LO frequency, but at the same time one could not so easily determine what that spacing actually is.

3. Technical considerations for SWIFTS

3.1. *Phase reference for the local oscillator*

The most crucial aspect of SWIFTS is the choice of the reference oscillator used for homodyne detection. Indeed, for a non-zero signal to be measured at all it must be the case that there is a definite phase relation between the optical beatnote and the reference oscillator. Otherwise, the phases will drift over laboratory timescales, resulting in an integrated signal of zero. (This is of course in contrast to beatnote interferometry, in which a signal can always be measured since spectrum analyzers operate in video detection mode.) In [2], a synthesizer was used as the reference, and the beatnote was phase-locked to the synthesizer by the application of low-frequency, low-current feedback in a phase-locked loop (PLL). This is made easier by the presence of a beatnote emanating directly from the QCL that is detectable on a bias tee [2, 23] or on an antenna [13], which effectively acts as a static detector on the QCL itself. Another way of forcing the repetition rate of the laser to the synthesizer frequency is by performing direct RF injection locking [8, 24]. However, this frequently has the side effect of reducing the coherence over the laser's operating bandwidth [1].

A third option is to forego the synthesizer altogether and to simply use the unstabilized beatnote of the QCL itself as a reference by taking it out of a bias tee, amplifying it, and using it as the LO for the I/Q demodulator. Provided the beatnote is still stable over short timescales, this *self-referenced* SWIFTS can still be used to assess coherence, albeit somewhat less rigorously. The real advantage for this reference, aside from its relative simplicity, is that it allows for the evaluation of QCLs whose outputs are not combs, including QCLs with multiple and broad beatnote regimes. In microresonator combs, such behavior was attributed to multiple lines existing in each resonator mode [26], but in QCLs it is also possible to imagine other behaviors arising from their rich dynamics. For example, voltage fluctuations on the laser could give rise to various pseudo-coherent regimes, in which the beatnote fluctuates over microsecond timescales but still has low timing jitter over even shorter timescales. Self-referenced SWIFTS therefore has the ability to probe the time-domain properties of lasers whose output is normally inaccessible to direct sampling techniques [8, 27, 28].

3.2. *Minimization of optical feedback*

An unfortunate property of many types of frequency combs is that their operation is extremely susceptible to optical feedback. This is especially problematic in QCL-based combs since essentially no low-loss optical isolators exist at mid-infrared and terahertz wavelengths. In the worst case scenario, transient feedback can even cause QCL combs to abruptly switch their mode of operation; Fig. 3(a) shows the spectrum of a THz QCL comb that abruptly switched from a comb regime to a single-mode regime due to a transient feedback event. Even when the effect is not quite so dramatic, feedback can cause PLLs to temporarily lose their lock on the beatnote, creating noise spikes in the SWIFTS measurement.

Clearly, minimizing the impact of feedback is critical for establishing the coherence of a comb. One of the major sources of feedback is frequently the presence of an FTS, which in commercial systems typically retroreflects a large fraction of a source's power. To make matters worse, the feedback is delay-dependent, so a laser that is stable at a particular FTS delay may

a   Effect of catastrophic feedback on comb

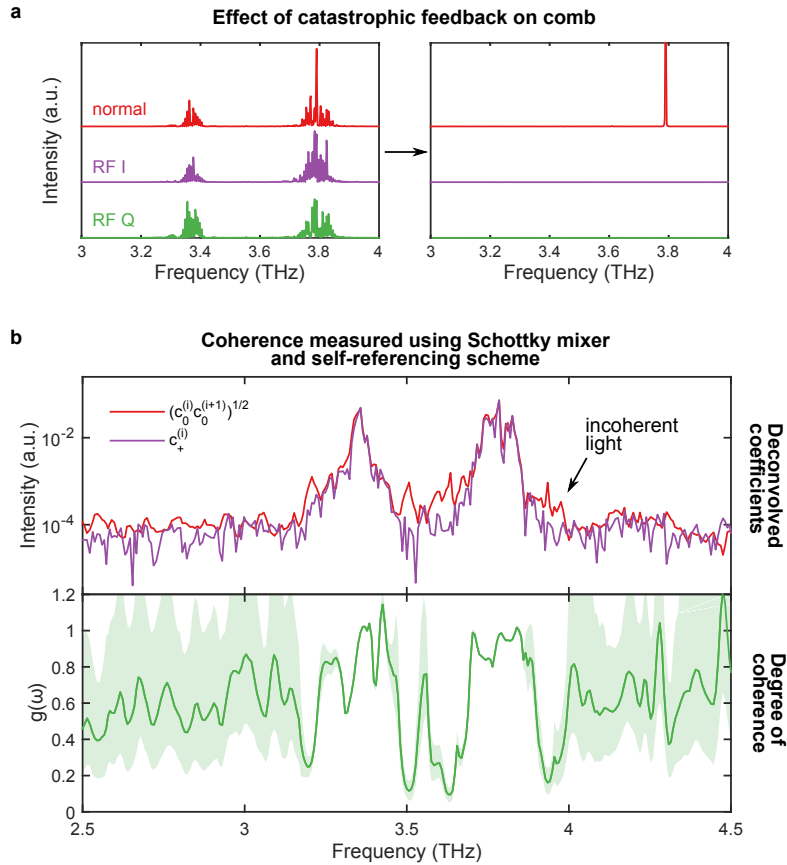**b**   Coherence measured using Schottky mixer and self-referencing scheme

Fig. 3. (a) Effect of transient feedback that destabilized comb operation and caused its output to become single-mode. The SWIFT signals vanish. (b) Coherence of a comb assessed without attenuation using a Schottky mixer and a self-referencing scheme. (Again, the shaded region represents a 95% confidence interval.) Feedback broadens the optical span but is detrimental to the coherence.

not be stable at another. The use of roof-type mirrors, as shown in Fig. 1(b), helps to prevent such retroreflection by ensuring that the reflected beam is spatially offset relative from the input one and can be blocked. Though this does not eliminate all feedback—in particular, feedback reflected from the detector itself—it does drastically reduce it. Attenuating the input beam can remove the residual feedback, but of course requires that a very sensitive detector be used.

Self-referenced SWIFTS can be used to assess coherence even in the case of moderate feedback, as the technique is relatively insensitive to the beatnote's center frequency. This permits the characterization of an unattenuated beam, which is attractive since it allows the use of less sensitive, uncooled detectors. Figure 3(b) shows the degree of coherence of an unattenuated THz QCL comb measured using a room-temperature VDI WR0.4XHM harmonic mixer from Virginia Diodes, with the comb operated at a temperature of 42 K and a bias of 899 mA. The power spectrum of the laser spans the full gain bandwidth of 800 GHz, but due to feedback the comb is actually not coherent over its full operating bandwidth: several holes in the degree of coherence are evident. This occurs despite the fact that the beatnote in this bias regime remains narrow. Great care must be taken when assessing the coherence of frequency combs, particularly when strong sources of feedback are present such as a spectrometer.

3.3. Calibration of the quadrature signals

The analysis of Section 2 implicitly assumed that perfect I/Q demodulators are used for SWIFTS detection. However, the quadrature LOs need not be completely orthogonal, just linearly independent. In other words, two mixers with a relative delay can be used instead, provided that the preceding analysis is modified. (This is more convenient at higher repetition rates, where broadband demodulators may not exist.) If the amplitude of the in-quadrature LO signal (Q) is A times the amplitude of the in-phase LO signal (I) and imparts a phase of ϕ, then the definitions of the analytic signals should be modified as follows:

$$S_\pm \equiv 2\frac{S_I - A^{-1}\exp(\mp i\phi)S_Q}{1 - \exp(\mp i2\phi)}. \tag{10}$$

Note that in the case of perfect demodulation $\phi = -\pi/2$ and $A = 1$, reducing to the previous definition of the analytic signals.

4. Extracting time-domain features from SWIFTS data

One of the attractive features of SWIFTS implied by its name is its ability to almost completely determine the time-domain behavior of an arbitrary comb, without relying on autocorrelation or any nonlinear detection element. This is a consequence of the fact that the deconvolved SWIFTS data effectively measures the phase difference between adjacent comb lines, since $\arg S_+(\omega) = \arg E(\omega + \Delta\omega) - \arg E(\omega)$. In fact, one can even argue that this is essentially the principle on which SWIFTS operates: multiplexed measurement of the phase difference of each comb pair.

As pointed out in [2], if SWIFTS is used to retrieve all of a comb's phase differences, then in principle it can be used to retrieve the full phase of the electric field by cumulative summing. Practically speaking, it might seem that noise and spectral gaps effectively make this an exercise in futility. Nevertheless, it is clearly the case that some information about the time-domain behavior is preserved, since the difference in adjacent lines is effectively group delay. If one can handle the noise in a statistical way, it is still possible to make inferences about the time-domain output. Figure 4 illustrates this by considering a thought experiment in which a comb has two lobes separated by a spectral gap. In this plot, the two lobes have different constant group delays—that is, they represent two pulses arriving at different times—but because the pulses overlap in the time domain the precise behavior of the time-dependent intensity is unknown, particularly in the region where the two pulses overlap. Nevertheless, there is clearly still information there: the regions where the pulses do not overlap is very well-determined, despite the unknown phase. Therefore, it is useful to calculate the statistics of the measurement, shown in the last panel, which shows the mean and standard deviation of the time-dependent intensity.

What time-dependent quantities are amenable to this sort of analysis? As it turns out, only quantities like the instantaneous intensity and frequency which are not particularly sensitive to global phase can be retrieved in this way. (An attempt to extract the instantaneous electric field, for example, would end poorly since statistical fluctuations overwhelm the measurement.) If an electric field has positive frequency components $E_+(t) = \sum_{\omega_i > 0} E_i \exp(i\omega_i t)$, then the instantaneous intensity and frequency can be defined respectively by

$$I(t) \equiv |E_+(t)|^2$$
$$f(t) \equiv \frac{1}{2\pi}\arg(E_+(t)) = \frac{1}{2\pi|E_+|^2}\mathrm{Im}\left[E_+^*\frac{dE_+}{dt}\right]. \tag{11}$$

(In the definition of frequency, an identity has been used that avoids discrete derivatives and phase unwrapping.) To make these quantities even more insensitive to phase fluctuations, it is
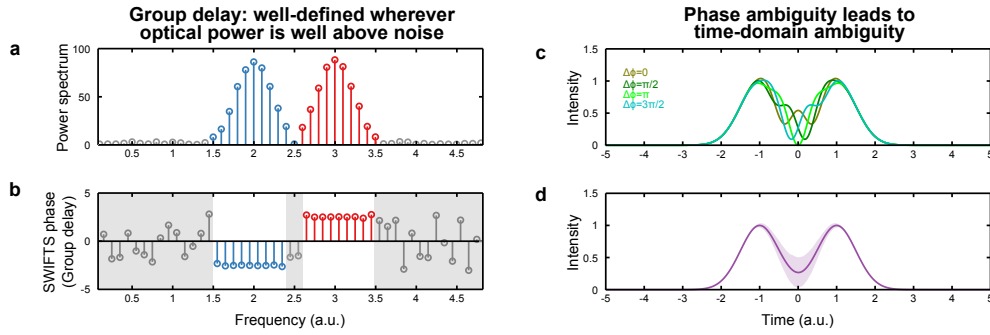
Fig. 4. (a) and (b): Hypothetical power spectrum and SWIFTS phase (group delay) of two time-domain pulses with a spectral gap between them, in the presence of noise. Though the phase is well-determined within a lobe, due to the gap the phase between the lobes is completely unknown. (c) Time-dependent intensity inferred by assuming various values of the relative phase. Despite the phase ambiguity, the intensities are nevertheless quite similar. (d) The corresponding distribution of intensities, with a standard deviation indicated by the shaded region (68% confidence interval).

often useful to filter them with a reasonable integration time (say 10 ps) to reduce the standard deviation of the measurement without filtering out potentially informative time-domain features. This reduces sensitivity to phase error since both $I(t)$ and $f(t)$ are comprised wholly of terms which go like $E_+^* E_+$, giving rise to a double summation over frequency differences. Filtering the data removes frequency differences that are large and are therefore more susceptible to statistical fluctuations.

Analytically calculating the statistics of the time-dependent quantities is challenging, and so Monte Carlo methods were used instead, according to the following procedure. First, regions of the measured spectra known to have no signal were used to generate a noise profile of each measured spectrum (i.e., normal, I, and Q). Then, at each frequency a possible value of the observed noise was drawn independently from this distribution, referred to as a noise instance. This instance was subtracted from the measurement, with the resulting signal effectively representing what the true signal might have been had it not been corrupted by noise. The deconvolution procedure previously described was used to find the spectral phasors, which were phase-corrected by the normal spectrum. Lastly, the SWIFT phases were cumulatively summed to find the phase of the electric field. Equation (11) was used to find the instantaneous intensity and frequency for the instance, and this process was repeated many times, allowing a distribution of $I(t)$ and $f(t)$ to be constructed.

Figure 5 shows the result of this process for the SWIFTS data shown in Fig. 2. The gain spectrum of this device has two distinct peaks, and so for ease of understanding the time-domain data is split into two portions. Lines represent mean values, and the shaded regions indicate a single standard deviation. First, consider the intensity versus time. The lower (red) lobe of the gain spectrum produces a time-domain pulse that arrives at t = 20 ps. Even though there is some uncertainty in the height of the pulse near its peak, it is clear that measurement noise does not prevent this conclusion. The upper (blue) lobe of the gain spectrum, meanwhile, lases at practically all times during the laser's period except for the time at which the red lobe is lasing. In other words, the red lobe only lases at times during which the upper lobe shuts off: its pulse-like behavior actually results from a type of temporal hole burning.

Shifting focus to the frequency versus time, note first that in each case the standard deviation of the frequency measurement grows large whenever the corresponding intensity is small, which is of course expected since the instantaneous signal-to-noise ratio (SNR) at these times
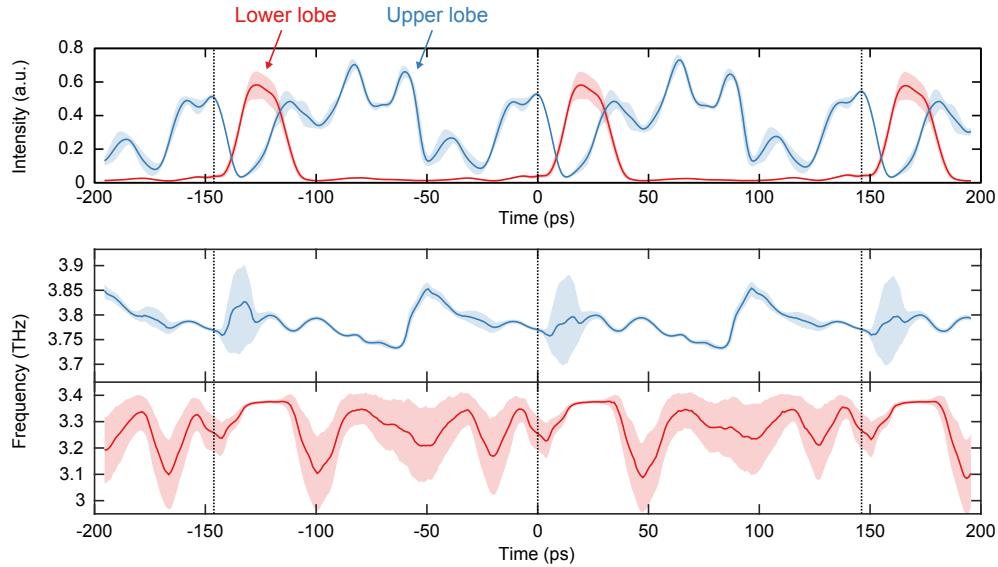
Fig. 5. Time-dependent intensity and frequency inferred from SWIFTS, filtered with a 10 ps window. Solid lines indicate the mean of the measurement, the shaded region indicates the standard deviation (68% confidence interval), and the dashed lines indicate a single repetition period (i.e., the round trip time).

is low. Next, note that the red lobe's frequency is essentially time-independent in the region in which its SNR is high, meaning that the pulse is not chirped and is nearly transform-limited. In contrast, the blue lobe is strongly frequency-modulated and has a sawtooth-like profile in the time-domain. It is interesting to note that the total intensity (red plus blue) is approximately constant in time, whereas the center frequency is strongly modulated. This analysis confirms that the type of behavior described in [9], in which four-wave mixing [29] leads to self-frequency modulation, can also occur in THz QCLs.

This information is extremely useful for characterizing the different regimes of comb operation, perhaps even more so than the frequency domain measurement alone. Figure 6 shows the bias dependence of $I(t)$ (measured using SWIFTS) alongside the different regimes of comb operation described in [2]. The three regions have strikingly different time-domain behavior. Region I is dominated by the red lobe, and exhibits a complicated multi-pulse emission. The blue lobe emits only when the red lobe transiently turns off; a signature of temporal hole burning is once again evident. In region III, the opposite occurs: the blue lobe dominates and the red lobe lases only when the blue one shuts off. In region II, the two signals have similar average powers, but the red lobe's power is concentrated in narrow time-domain pulses while the blue lases nearly continuously. It is a regime of strong amplitude modulation (AM) rather than frequency modulation (FM), and may be in a regime of quasi-active mode-locking, in which the presence of a comb in the cavity leads to a beatnote sufficiently strong to enforce a pulse condition.

5. Conclusion

We have clarified the issues surrounding QCL comb coherence and shown how high-speed linear detectors can be used to measure the mutual coherence of such combs without relying on nonlinear processes. In doing so, we have presented a directly-measureable quantity that evaluates their performance. We also discussed many of the technical issues surrounding the
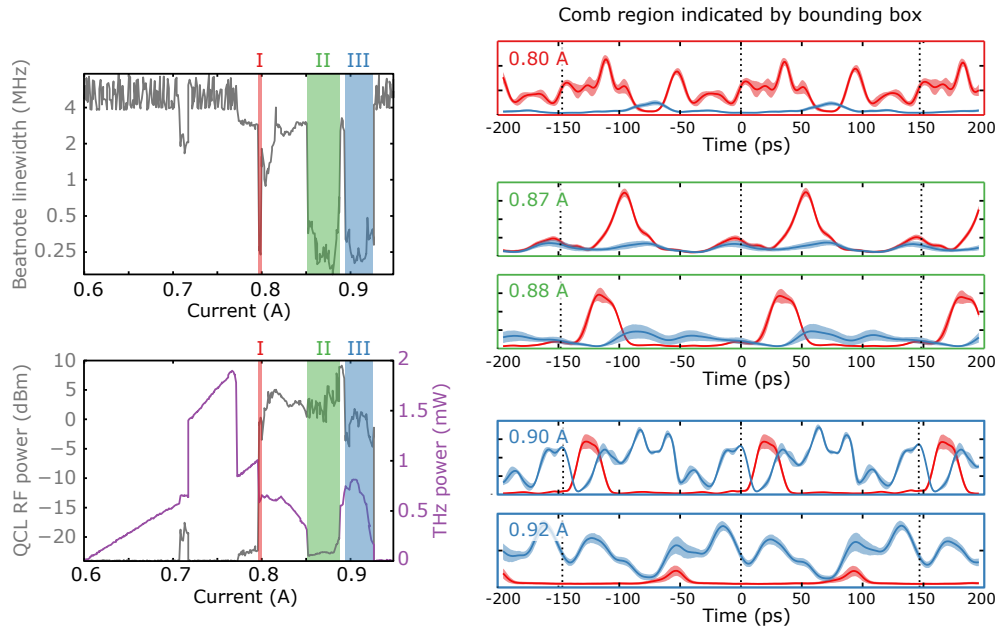
Fig. 6. Bias dependence of time-dependent intensities of a THz comb at 50 K (right panels). Red represents lower lobe frequencies and blue represents upper lobe frequencies. Upper left panel: beatnote linewidth versus bias. Bottom left panel: beatnote power (measured from QCL) and THz power versus bias.

implementation of the SWIFTS technique, and have shown how such measurements can be used to elucidate the time-domain properties of arbitrary combs.

Acknowledgments